ACSNANO

www.acsnano.org

ARTICLE

DNA Hairpins and Dumbbell-Wheel Transitions Amplified Walking Nanomachine for Ultrasensitive Nucleic Acid Detection

Peng Miao,* Hua Chai, and Yuguo Tang

Cite This: *ACS Nano* 2022, 16, 4726–4733

Read Online

ACCESS | Metrics & More | Article Recommendations | Supporting Information

ABSTRACT: Nucleic acids, including circulating tumor DNA (ctDNA), microRNA, and virus DNA/RNA, have been widely applied as potential disease biomarkers for early clinical diagnosis. In this study, we present a concept of DNA nanostructures transitions for the construction of DNA bipedal walking nanomachine, which integrates dual signal amplification for direct nucleic acid assay. DNA hairpins transition is developed to facilitate the generation of multiple target sequences; meanwhile, the subsequent DNA dumbbell-wheel transition is controlled to achieve the bipedal walker, which cleaves multiple tracks around electrode surface. Through combination of strand displacement reaction and digestion cycles, DNA monolayer at the electrode interface could be engineered and target-induced signal variation is realized. In addition, pH-assisted detachable intermolecular DNA triplex design is utilized for the regeneration of electrochemical biosensor. The high consistency between this work and standard quantitative polymerase chain reaction is validated. Moreover, the feasibilities of this biosensor to detect ctDNA and SARS-CoV-2 RNA in clinical samples are demonstrated with satisfactory accuracy and reliability. Therefore, the proposed approach has great potential applications for nucleic acid based clinical diagnostics.

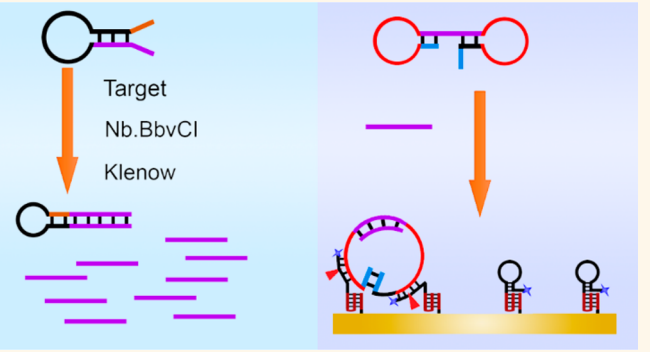

KEYWORDS: *circulating tumor DNA, SARS-CoV-2 RNA, DNA walker, strand displacement amplification, biosensors*

INTRODUCTION

Nucleic acids contain significant biological information for understanding physiologic and pathological states.[1,2] The levels of specific sequences can be applied as important indicators of a variety of diseases.[3] For example, circulating tumor DNA (ctDNA) is a type of cell-free DNA fragments derived from malignant cells, which carries tumor-specific sequence alterations.[4] SARS-CoV-2 RNA testing of respiratory samples is an important way to prevent and control the coronavirus disease 2019 (COVID-19) pandemic.[5] Accurate determination of the concentrations of target DNA or RNA plays a critical role in the diagnosis and prognosis of certain diseases, which should be intensively investigated.[6,7] Based on the definite Watson–Crick base pairing principle, nucleic acid analysis can be achieved by converting hybridization information into detectable signals like commonly used fluorescence.[8,9] Currently, standard techniques for the quantification of nucleic acid include classical polymerase chain reaction (PCR), digital PCR (dPCR),[10] microarray,[11] next-generation sequencing (NGS),[12] mass spectrometry,[13] and so on. However, the requirements of complicated equipment, expensive reagents, and tedious reaction steps restrict their wide applications in clinical scenes. In order to overcome the limitations, different techniques have been under development. For example, Wang et al. developed a fluorescence lateral assay for the detection of SARS-CoV-2 RNA by the employment of monoclonal antibody toward DNA–RNA hybrids.[14] Fan's group engineered various tetrahedral DNA nanostructures on gold electrode for sensitive electrochemical detection of DNA.[15] Xue et al. fabricated a surface plasmon resonance method for specific microRNA assay based on two-dimensional nanomaterial of antimonene.[16]

To achieve better analytical performances, signal amplification, especially isothermal exponential amplification strategies

Received: December 28, 2021
Accepted: February 18, 2022
Published: February 21, 2022

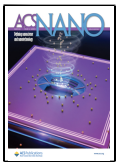

https://doi.org/10.1021/acsnano.1c11582
ACS Nano 2022, 16, 4726–4733

Scheme 1. Illustration of the Electrochemical Sensing Strategy for the Detection of Nucleic Acid

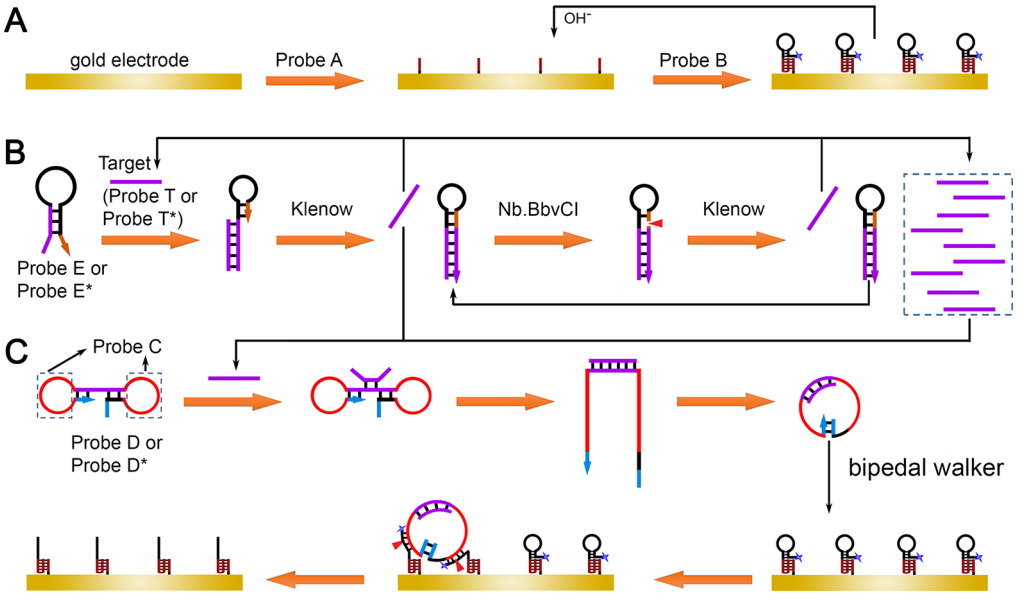

have attracted great attention in the development of nucleic acid detection systems.[17,18] Rolling circle amplification (RCA),[19] hybridization chain reaction (HCR),[20] strand displacement amplification (SDA),[21] loop-mediated amplification (LAMP),[22] and catalytic-hairpin assembly (CHA)[23] have been widely studied and integrated in various biosensors. Among them, SDA exhibits outstanding amplification capability with a number of replicated DNA strands generated from Target.[24,25] Besides, DNA nanomachine is a type of artificial molecular device inspired by nature.[26,27] The nanoscale mechanical motion can be precisely controlled, which contributes to the generation of amplified signal.[28] A number of DNA nanomachines with various functionalities have been constructed including DNA walker,[29] gear,[30] and tweezer,[31] which have great potential in biomedical applications.

In this study, we have pioneered a DNA bipedal walker with dumbbell-wheel structural transition for nucleic acid detection, which is further amplified by DNA hairpins transition-mediated SDA. ctDNA is first taken as an example Target input, which is a promising noninvasive tumor biomarker.[32] A hairpin structured DNA combining the primer and template sequences of SDA is designed to improve the reaction efficiency. Target sequence is able to assist the formation of a more stable hairpin for fast SDA and the generated multiple products are responsible for the DNA dumbbell-wheel transition. Downstream bipedal walking is then carried out on the electrode surface and ultrahigh sensitivity for Target assay is achieved.

RESULTS AND DISCUSSION

Sensing Principle of the Electrochemical Method. We have established a reusable electrode interface for the biosensor. As shown in Scheme 1A, a pH-controlled detachable intermolecular DNA triplex nanostructure is constructed between DNA Probe A and B (Supporting Information (SI) Figure S1A).[33] Single-stranded Probe A with multiple cytosine bases is first attached on the gold electrode surface via gold−sulfur chemistry.[34] The hairpin-structured Probe B can be further immobilized by the Hoogsteen interaction between its stem segment and cytosine-rich segment of Probe A.[35] The immobilized Probe B can be easily released by alkaline treatment which destroys the Hoogsteen interaction. Also, regeneration of Probe A/B modified electrode can be facilely achieved by adjusting the pH condition and subsequent incubation with fresh Probe B. The regeneration procedure not only promises high stability, but also reduces the cost for point-of-care testing applications.

Next, we have designed a simple but effective SDA strategy to amplify Target sequences. Allele of KRAS gene as ctDNA (Probe T) is first introduced as an example (SI Table S1). As shown in Scheme 1B, another hairpin-structured Probe E is designed, which integrates primer and template sequences for SDA into one. This smart form improves the reaction efficiency compared with traditional SDA with discrete primer and template design.[36] A short single-stranded segment at the 5′ end is applied as a toehold for Target nucleic acid binding. After specific recognition, the loop of Probe E is opened. The unrestrained single-stranded segment at the 3′ end can thus hybridize with part of original loop sequence, leading to the formation of another hairpin structure. In addition, the segment even acts as the primer and extension is catalyzed with Klenow fragment polymerase. Target sequence can thus be released and recycled. Since a restriction site of nicking endonuclease is designed in the stem section of the newly formed hairpin, after further introducing Nb.BbvCI, a nick is created, followed by multiple rounds of polymerization and strand displacement. The generated single-stranded DNAs contains Probe T sequence, which are applied for following reactions.

A DNA wheel based bipedal walker is then developed which is initiated by the above SDA products. As depicted in Scheme 1C, the loop parts of dumbbell-structured Probe D contains the red parts of DNAzyme sequences (Probe C) which are inactivated in original state. However, the stem part interacts with Probe T sequence from SDA and relieves the two loops. Self-hybridization in turn occurs between the 5′ and 3′ terminals of Probe D. A DNA wheel structure is thus formed by Probe D/T. Before interacting with electrode interface, the pH condition is controlled to satisfy the requirements of triplex nanostructure. The DNA wheel contains active Probe C

https://doi.org/10.1021/acsnano.1c11582
ACS Nano 2022, 16, 4726−4733

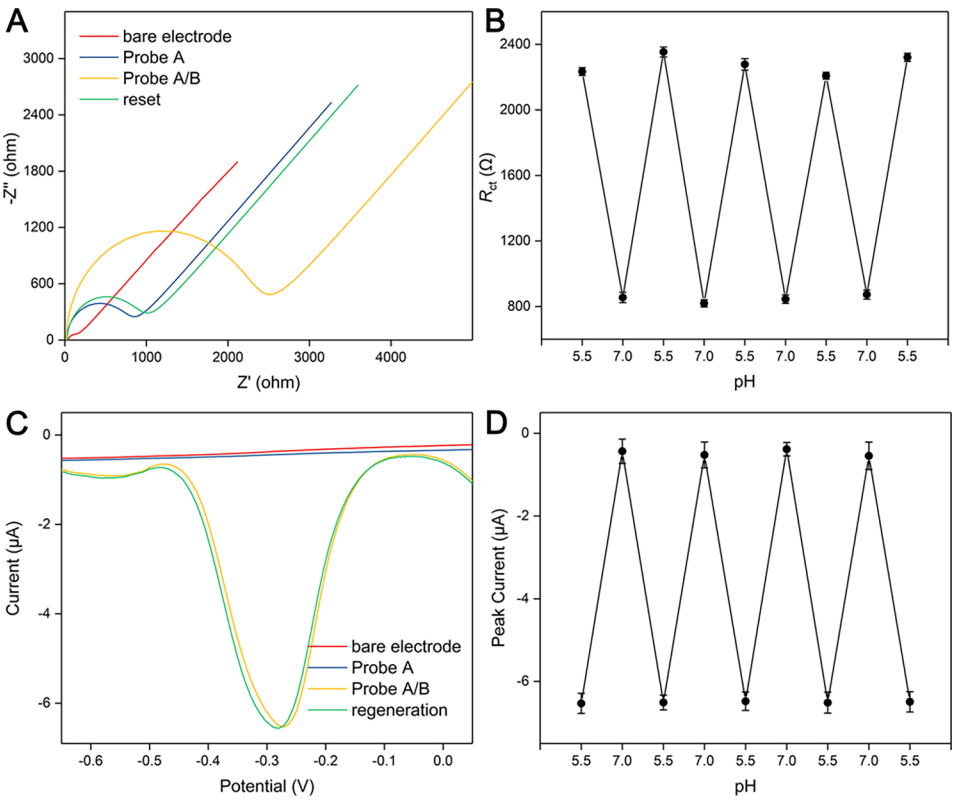

Figure 1. (A) Nyquist plots corresponding to bare electrode, Probe A modified electrode, Probe A/B modified electrode, after alkaline treatment. (B) R_{ct} values of DNA modified electrode after cyclically changing pH between 5.5 and 7.0. (C) Square wave voltammograms corresponding to bare electrode, Probe A modified electrode, Probe A/B modified electrode, after regeneration of electrode by changing pH. (D) SWV peak currents of DNA modified electrode after cyclically changing pH between 5.5 and 7.0.

sequences for bipedal walking. After interacting with adjacent Probe B at the electrode surface, DNAzyme-catalyzed cleavage reactions occur with the existence of suitable cofactors. The release of electrochemical tracer modified at the 5′ end of Probe B explains the decrease of the electrochemical response. In addition, DNA wheel with bipedal walking strands could move around the surface of electrode to cleave more Probe B strands. By analyzing the electrochemical responses, Target concentration can be evaluated. To probe different Targets, only slight adjustments of Probe D and E are required. Generally, the complementary sequences of Target (purple parts) are displaced according to new Target; meanwhile, the stems (black and blue parts) should also be altered to fulfill complementary hybridization. Note that, due to the existence of duplex part of Target/Probe D, circularization can be formed with the Target length less than 70 nt.

Confirmation of DNA Nanostructure Transitions. The feasibility of the sensing strategy relies on the control of DNA nanostructures, which is first theoretically analyzed. DNA melting temperature (T_m) during transitions is applied as an important parameter. Higher T_m indicates a steadier state. We have calculated T_m values of two hairpins as well as dumbbell and wheel structured DNA. The obtained values demonstrate the thermodynamically tendencies of DNA transitions (SI Figure S1B).

Gel electrophoresis is then performed to analyze the reactants and products during the transitions. For hairpins transition based SDA, after the hybridization between Target and Probe E, the original hairpin of Probe E is reconstructed with a larger molecule weight, which is supposed to run slower in the gel. The band position is observed to be higher, demonstrating successful hairpins transition (lane c, SI Figure S2A). After further introduction of polymerase, Target is displaced and a complete new hairpin structure is formed (lane d). Dimer of the polymerized product may be assembled. However, the yield is quite low and the band can hardly be observed. After further introduction of nicking endonuclease, multiple single-stranded DNA containing Target sequence are generated, which is located at the band above the displaced Target band (lane e). We have then studied DNA dumbbell-wheel transition and walking reactions by gel electrophoresis. After reaction between Target and Probe D, the product runs slower than Probe D and the band reflects a higher molecule weight (lane a and b, SI Figure S2B). On the contrary, after mixing Probe B and D in the presence of Mg^{2+}, the position of the resulting bands are identical to single Probe B and D (lane d). It is because the DNAzyme sequences are restricted in the loops of Probe D, inhibiting effective hybridization with Probe B. We have then drawn out DNAzyme sequence (Probe C) from Probe D to demonstrate the cleavage activity.[37] After incubating Probe C with Probe B in the presence of Mg^{2+}, the band of Probe B disappears, and two new bands with smaller molecule weights are observed, which are ascribed to the cleaved products of Probe B (lane f). We have further challenged the Probe D/T in the digestion of Probe B. Similar results are achieved compared with the case of Probe C, suggesting effective structural transition of Probe D to activate DNAzyme (lane e).

Electrochemical Characterizations. DNA assembly at electrode surface is first characterized by chronocoulometry

https://doi.org/10.1021/acsnano.1c11582
ACS Nano 2022, 16, 4726−4733

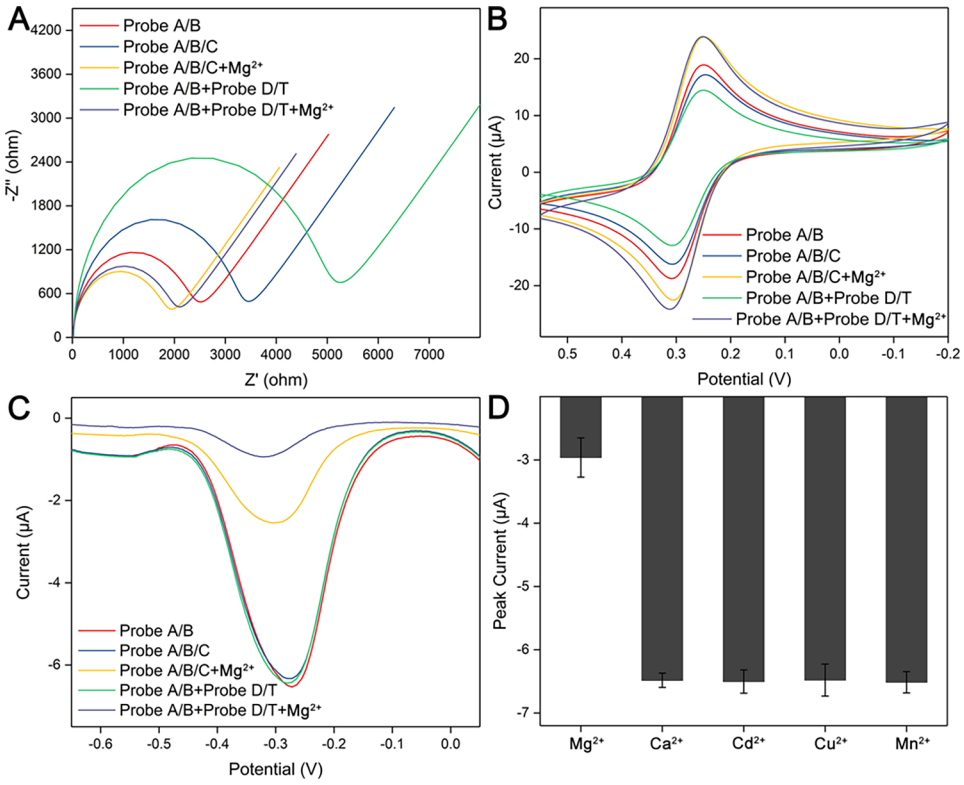

Figure 2. (A) Nyquist plots, (B) cyclic voltammograms and (C) square wave voltammograms of Probe A/B modified electrode, after Probe C or Probe D/T immobilizations in the absence and presence of Mg^{2+}. (D) SWV peak currents of the sensing system with the cofactors of Mg^{2+}, Ca^{2+}, Cd^{2+}, Cu^{2+}, and Mn^{2+}, respectively.

(CC). After incubating 0.8 μM Probe A with the electrode, a large number of hexaammineruthenium(III) chloride ($[Ru(NH_3)_6]^{3+}$) can be adsorbed on the DNA strand. After investigating the CC curve (SI Figure S3), the DNA coverage density at the electrode interface is determined according to Cottrell equation, which is estimated to be 1.9 pmol/cm^2.[38] We have then applied electrochemical impedance spectroscopy (EIS) and square wave voltammetry (SWV) to check the regeneration of the electrode interface. As shown in Figure 1A, after the incubation with Probe A, the electrochemical species of $[Fe(CN)_6]^{3-/4-}$ could be repelled by the negatively charged DNA monolayer.[39] Therefore, a semicircle domain appears in the nyquist plot, replacing the straight line for bare electrode. After further interaction with Probe B, the intermolecular DNA triplex on the electrode shows larger negativity thus the diameter of the semicircle domain becomes larger. However, after controlling the pH condition, excess Probe B strands can be disassociated and the nyquist plot recovers to the state of original Probe A modified electrode. We have then estimated charge transfer resistance (R_{ct}) values of the DNA modified electrode with different pH conditions, which indicates pH control is a promise way to repeatedly adjust DNA assembly states on electrode surface (Figure 1B). We have also studied the detachability of triplex DNA structure by measuring SWV signal of methylene blue (MB) labeled at the end of Probe B. As shown in Figure 1C, no current peaks are observed for bare electrode and Probe A modified electrode. After incubation with Probe B, the labeled MB contributes to the significant current peak around −0.3 V. After resetting the electrode by alkaline treatment and regeneration by fresh Probe B incubation, the peak current can be successfully recovered. By cycles of regeneration, the peak current barely changes, demonstrating excellent stability of the treatment (Figure 1D).

The properties of electrode during different experimental stages are investigated by EIS, cyclic voltammetry (CV) and SWV. As shown in Figure 2A, after incubating Probe C with Probe A/B modified electrode, the semicircle domain is enlarged, verifying successful hybridization reaction. However, after introduction of cofactor Mg^{2+}, DNAzyme is activated to cleave Probe B and the semicircle diameter is decreased. Similar trends are achieved by successively introducing Probe D/T and Mg^{2+}, demonstrating that bipedal walker can be carried out like monopedal walker. Figure 2B are corresponding CV curves. The changes of peak currents are consistent with the variations of R_{ct} values in Figure 1A. The SWV curves recorded in Figure 2C also indicate that Mg^{2+} is essential for the cleavage reactions. Note that the concentrations of introduced Probe C and Probe T are the same. However, with bipedal walking (Probe D/T), the SWV peak variation is much larger than that of pure Probe C assisted monopedal walker. It reflects the high efficiency of upstream SDA that generates abundant strands to activate more Probe C regions on bipedal walker. We have then introduced other metal ions as potential cofactors for DNAzyme including Ca^{2+}, Cd^{2+}, Cu^{2+}, and Mn^{2+}. After referring to the SWV peak currents, none of them participate in the cleavage reactions and the finally obtained peaks are nearly unchanged (Figure 2D). Therefore, it is concluded that the applied DNAzyme sequences are only sensitive to Mg^{2+}.

Optimization of Experimental Conditions and Electrochemical Quantification. To improve the detection sensitivity, several parameters should be studied throughout. By comparing the finally recorded SWV peak currents, the

https://doi.org/10.1021/acsnano.1c11582
ACS Nano 2022, 16, 4726−4733

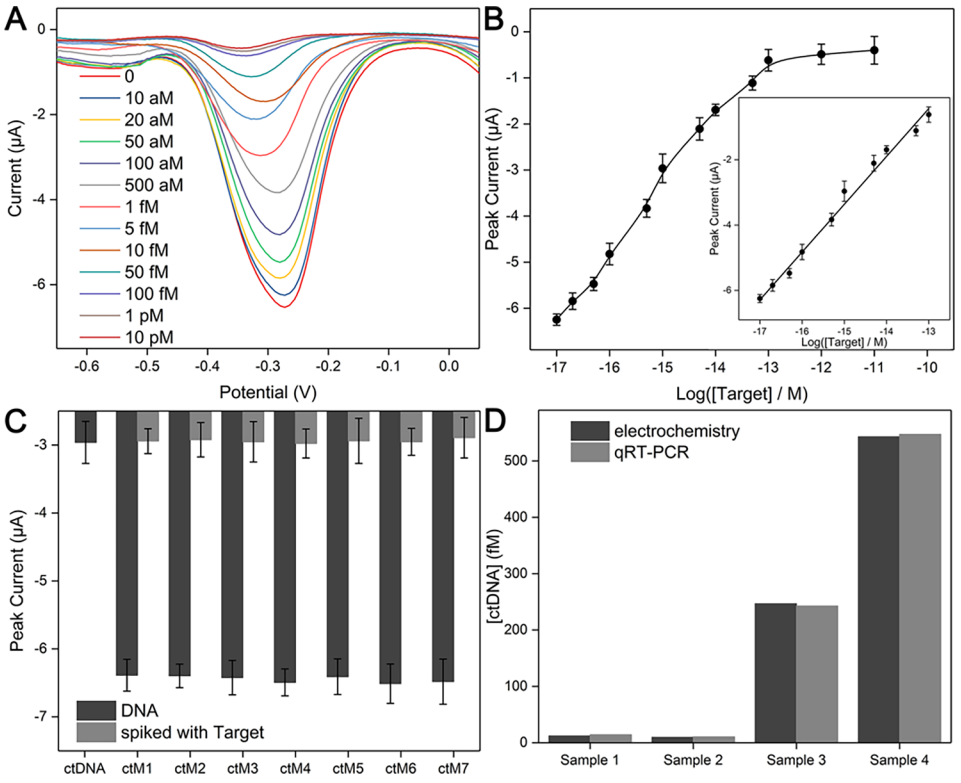

Figure 3. (A) Square wave voltammograms of the sensing system for the detection of ctDNA with the concentrations: 0, 10^{-17}, 2×10^{-17}, 5×10^{-17}, 10^{-16}, 5×10^{-16}, 10^{-15}, 5×10^{-15}, 10^{-14}, 5×10^{-14}, 10^{-13}, 10^{-12}, 10^{-11} M. (B) Calibration curve reflecting the relationship between ctDNA concentration and peak currents. Inset shows the linear range. (C) SWV peak currents for the detection of Target (1 fM) and mismatched sequences (10 fM). (D) Detection of ctDNA in random serum samples by the proposed electrochemical method and qRT-PCR assay.

optimized conditions are as follows: 0.8 μM Probe A, 0.2 μM Probe D, and 30 mM Mg^{2+} (SI Figure S4A–C). We have also compared the kinetics of monopedal (Probe C) and bipedal walking (Probe D/T). Since the DNA wheel structure contains two legs for walking, the cleavage reaction can be accomplished in 15 min, which is one-quarter of that for monopedal walking, demonstrating improved reaction efficiency (SI Figure S4D). Under these optimized conditions, the performances of the electrochemical biosensor for the detection of Target nucleic acid are studied. As shown in Figure 3A, SWV peak decreases with Target concentration increased from 10 aM to 10 pM. The peak currents for independent measurements of different concentrations of Target are recorded. The relative errors are less than 7%, indicating good reproducibility of this approach. Detailed relationship between peak current and logarithm of Target concentration is depicted in Figure 3B. A wide linear range is established from 10 aM to 100 fM with the equation as follows:

$$y = 18.592 + 1.464x (n = 3, R^2 = 0.993)$$

in which y stands for the measured SWV peak current and x is the logarithm of Target concentration. The limit of detection is calculated to be 2.2 aM (S/N = 3). Since multiple reaction procedures are integrated to improve the sensitivity, overall testing time is relatively long. However, compared with previously developed strategies, this work exhibits ultrahigh sensitivity, indicating obvious analytical superiority (SI Table S2). The linear range is satisfactory for biological studies and clinical diagnosis. The excellent performances are ascribed to the upstream SDA to produce walking trigger strands and downstream bipedal walker for efficient engineering of tracks on electrode surface.

Investigation of Selectivity and Practical Utility. To check the selectivity of the electrochemical biosensor, seven DNA sequences with various mismatched sites are chosen as potential interferents. As shown in Figure 3C, the recorded SWV peaks with the cases of mismatched strands are quite large, indicating the absence of DNA walking to eliminate MB from the electrode surface. However, after spiking certain levels of Target, sharp declines of peak currents are achieved, which are identical to the response of single Target ctDNA. These results are solid evidence to support the high selectivity of this method. To primarily investigate its feasibility in real biological samples, we have first determined Target concentrations in four random clinical serum samples by comparing the SWV peaks with the established calibration curve. As shown in Figure 3D, the measured concentrations by the proposed method are quite consistent with standard qRT-PCR, demonstrating excellent accuracy of the proposed electrochemical biosensor.

Probe A/B modified electrodes are also demonstrated to be highly stable. After stored in 4 °C for 2 weeks, the electrochemical response maintains over 94% compared with freshly prepared electrodes, suggesting promising practical utility. We have further introduced grouped clinical samples collected from healthy individuals and breast cancer patients. Peripheral blood samples are first collected. After centrifugation, serums are diluted for 10 folds with 10 mM Tris-HCl. The applied buffer dilutes possible interfering molecules or enzymes in the serum, which also supplies suitable pH and

https://doi.org/10.1021/acsnano.1c11582
ACS Nano 2022, 16, 4726–4733

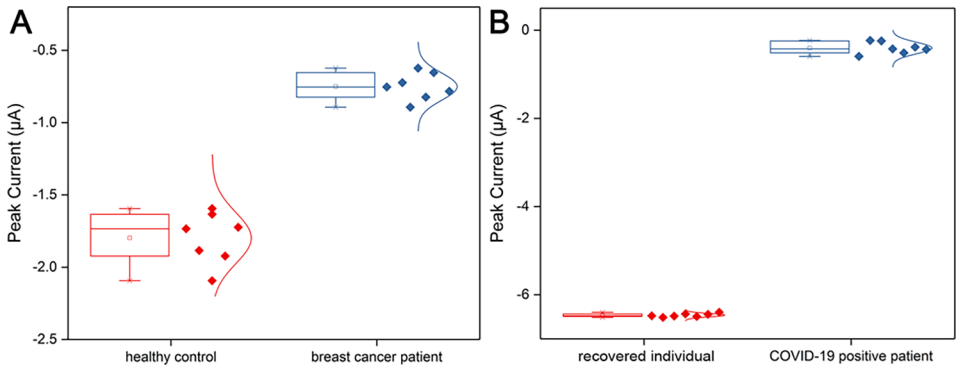

Figure 4. Box plots of SWV peak intensities for (A) breast cancer patients and healthy controls, (B) COVID-19 positive patients and recovered individuals.

ionic environment for DNA hybridizations. Afterward, the ctDNA levels are directly evaluated by the proposed method. As revealed in Figure 4A, the obtained SWV peak currents for patients are significantly higher than those for healthy controls, which are due to the existence of overexpressed ctDNA that initiates DNA walker. To further assess the clinical applicability, we have modified the DNA sequences (Probe D* and E*) in this study to adapt to SARS-CoV-2 RNA (Probe T*). After careful treatments of oropharyngeal swabs of COVID-19 positive patients and recovered individuals, total RNAs (at least 100 ng for the following experiments) are extracted with a nucleic acid isolation kit from Bioperfectus Technologies (Taizhou, China). After analyzed by the proposed method, the electrochemical responses are displayed in Figure 4B. It is clearly observed that the differences of electrochemical responses for the patients and controls are even larger. It is due to the fact that there are nearly no exogenous virus RNAs in recovered individuals, whereas the RNAs are heavily replicated in positive patients. Detailed information about calculated nucleic acids concentrations can be found to be consistent with qRT-PCR results, further demonstrating good accuracy of this strategy when challenging real samples (SI Table S3).

CONCLUSION

In summary, we present a DNA nanostructure transitions-based DNA bipedal walker to identify Target nucleic acid sequence. Dual amplification via successive SDA and walking nanomachine promises ultrahigh sensitivity. With nanoscale control of DNA structural transitions, high selectivity can be validated. Traditional bipedal walking nanomachine usually requires multiple single-stranded DNA probes as walking strands. The design of the proposed wheel structured bipedal walker is facile and concise, which releases two reaction regions hidden inside original dumbbell structured DNA. The as-prepared electrochemical method not only couples cascade reactions to achieve exponential amplification dynamics, but also takes full advantage of pH-controlled detachable intermolecular DNA triplex for regeneration. Thus, repeated modification of the electrode can be avoided and the cost-effective detection is reliable. Upon the application of optimized experimental conditions, the proposed method offers a limit of detection as low as 2.2 aM and excellent single base resolution. Moreover, different kinds of Targets including ctDNA and SARS-CoV-2 RNA have been tested in clinical samples with satisfactory results. The strategy could also be extended to other Targets with different GC contents by simply adjusting Probe D and E accordingly. Therefore, the electrochemical biosensor can be utilized as a promising tool for nucleic-acid-based clinical disease screening which has important significance to public health administration.

EXPERIMENTAL SECTION

Materials and Chemicals. Tris(2-carboxyethyl)phosphine hydrochloride (TCEP), ethylenediaminetetraacetic acid (EDTA), sodium hydroxide (NaOH), mercaptohexanol (MCH), and $[Ru(NH_3)_6]^{3+}$ were ordered from Sigma-Aldrich (U.S.). Klenow fragment, Nb.BbvCI, and dNTPs were obtained from New England Biolabs, Ltd. (Beijing, China). Human serum and oropharyngeal swab samples were supplied by local hospitals (China). Informed written consent from all participants was obtained prior to the research. All protocols involving human subjects were previously approved by the Ethics Committee for the Use of Human Subjects of Second Hospital of Nanjing. All other chemicals were of analytical grade and used as received. Solutions prepared in this study utilized DEPC treated redistilled deionized water. All oligonucleotides were synthesized and purified by Sangon Biotech Co., Ltd. (Shanghai, China). The sequences are listed in SI Table S1.

Preparation of Probe A/B Immobilized Gold Electrode. The substrate gold electrode was cleaned prior to modification. Briefly, the electrode was incubated with piranha solution for about 5 min (*Caution: Piranha solution dangerously attacks organic matter!*). Next, it was rinsed with double-distilled water and then carefully polished (silicon carbide paper and alumina powders with diameters of 1.0, 0.3, 0.05 μm). Subsequently, the gold electrode was sonicated in ethanol and then double-distilled water for 5 min. It was further electrochemically cleaned by employing 0.5 M H_2SO_4. The cleaned electrode was incubated with Probe A (0.8 μM, 10 mM Tris-HCl, 1 mM EDTA, 10 mM TCEP, and 0.1 M NaCl, pH 7.4) for 8 h and then MCH for 30 min. After carefully rinsing, the electrode was further incubated with Probe B (1 μM, 10 mM phosphate buffer, 250 mM NaCl, pH 5.7) for 1 h.

DNA Hairpins Transition Based SDA. 50 μL of sample that contains Target sequence was mixed with 10 μL of Probe E (1 μM), 2 μL of Klenow fragment, 3 μL of Nb.BbvCI, 25 μL of dNTPs (2.5 mM) and 10 μL of 10 × NEB buffer 2.1. After reacting at 37 °C for 2 h, the enzymes were inactivated by heating to 80 °C for 20 min.

DNA Dumbbell-Wheel Transition for Walking and Electrochemical Measurements. The above solution was further blended with Probe D (1.5 μM) and Mg^{2+} (30 mM). pH of the solution was adjusted to 5.5. Probe A/B modified electrode was incubated with the solution for 15 min. After that, electrochemical measurements were performed using a CHI 660D electrochemical workstation (CH Instrument, China). A three-electrode system was assembled applying a saturated calomel reference electrode (SCE), a platinum auxiliary electrode, and the reacted gold working electrode. CV and EIS were carried out in the electrolyte of 5 mM $[Fe(CN)_6]^{3-/4-}$ with 1 M KNO_3. CC was carried out in 10 mM Tris−HCl solutions containing

https://doi.org/10.1021/acsnano.1c11582
ACS Nano 2022, 16, 4726−4733

50 μM $[Ru(NH_3)_6]^{3+}$ while SWV was performed in 20 mM Tris-HCl. The scan ranges for CV and SWV were 0.55 to −0.2 V and −0.65 to 0.05 V, respectively. The parameters for EIS were 0.21 V biasing potential, 5 mV amplitude, and 0.1 Hz to 100 kHz frequency range.

Electrophoresis Measurements. Polyacrylamide gel electrophoresis was performed in the Tris-boric acid buffer solution (90 mM, 1 mM EDTA, pH 8.0) at 110 V for 50 min. Then, the polyacrylamide gel was stained with 4S Red Plus solution, which was further photographed under UV light by Gel DocTM XR+ Imaging System (Bio-Rad, U.S.).

ASSOCIATED CONTENT

Supporting Information

The Supporting Information is available free of charge at https://pubs.acs.org/doi/10.1021/acsnano.1c11582.

Detailed interaction between Probe A and B; T_m values of DNA nanostructures; polyacrylamide gel electrophoresis analysis of reaction processes; chronocoulometry curves for DNA modified electrodes; optimizations of experimental reactions; DNA and RNA sequences; comparison of analytical performances; detailed concentration information determined by qRT-PCR and the proposed biosensor (PDF)

AUTHOR INFORMATION

Corresponding Author

Peng Miao − *University of Science and Technology of China, Hefei 230026, China; Suzhou Institute of Biomedical Engineering and Technology, Chinese Academy of Sciences, Suzhou 215163, People's Republic of China;* orcid.org/0000-0003-3993-4778; Email: miaopeng@sibet.ac.cn

Authors

Hua Chai − *University of Science and Technology of China, Hefei 230026, China; Suzhou Institute of Biomedical Engineering and Technology, Chinese Academy of Sciences, Suzhou 215163, People's Republic of China*

Yuguo Tang − *University of Science and Technology of China, Hefei 230026, China*

Complete contact information is available at: https://pubs.acs.org/10.1021/acsnano.1c11582

Notes

The authors declare no competing financial interest.

ACKNOWLEDGMENTS

This work is supported by the Science and Technology Cooperation Project between the Chinese and Australian Governments (Grant No. 2017YFE0132300), the Natural Science Foundation of Jiangsu Province (Grant no. BK20201184), and the Basic Research Program of Suzhou (Grant no. SJC2021016).

REFERENCES

(1) Mertens, J.; Rogero, C.; Calleja, M.; Ramos, D.; Martín-Gago, J. A.; Briones, C.; Tamayo, J. Label-free Detection of DNA Hybridization Based on Hydration-induced Tension in Nucleic Acid Films. *Nat. Nanotechnol.* **2008**, *3*, 301−307.

(2) Ho, N. R. Y.; Lim, G. S.; Sundah, N. R.; Lim, D.; Loh, T. P.; Shao, H. Visual and Modular Detection of Pathogen Nucleic Acids with Enzyme-DNA Molecular Complexes. *Nat. Commun.* **2018**, *9*, 3238.

(3) Tavallaie, R.; McCarroll, J.; Le Grand, M.; Ariotti, N.; Schuhmann, W.; Bakker, E.; Tilley, R. D.; Hibbert, D. B.; Kavallaris, M.; Gooding, J. J. Nucleic Acid Hybridization on an Electrically Reconfigurable Network of Gold-coated Magnetic Nanoparticles Enables microRNA Detection in Blood. *Nat. Nanotechnol.* **2018**, *13*, 1066−1071.

(4) Zhu, G.; Guo, Y. A.; Ho, D.; Poon, P.; Poh, Z. W.; Wong, P. M.; Gan, A.; Chang, M. M.; Kleftogiannis, D.; Lau, Y. T.; Tay, B.; Lim, W. J.; Chua, C.; Tan, T. J.; Koo, S.-L.; Chong, D. Q.; Yap, Y. S.; Tan, I.; Ng, S.; Skanderup, A. J. Tissue-specific Cell-free DNA Degradation Quantifies Circulating Tumor DNA Burden. *Nat. Commun.* **2021**, *12*, 2229.

(5) Ning, B.; Huang, Z.; Youngquist, B. M.; Scott, J. W.; Niu, A.; Bojanowski, C. M.; Zwezdaryk, K. J.; Saba, N. S.; Fan, J.; Yin, X.-M.; Cao, J.; Lyon, C. J.; Li, C.-z.; Roy, C. J.; Hu, T. Y. Liposome-mediated Detection of SARS-CoV-2 RNA-positive Extracellular Vesicles in Plasma. *Nat. Nanotechnol.* **2021**, *16*, 1039−1044.

(6) Bloom, J. S.; Sathe, L.; Munugala, C.; Jones, E. M.; Gasperini, M.; Lubock, N. B.; Yarza, F.; Thompson, E. M.; Kovary, K. M.; Park, J.; Marquette, D.; Kay, S.; Lucas, M.; Love, T.; Sina Booeshaghi, A.; Brandenberg, O. F.; Guo, L.; Boocock, J.; Hochman, M.; Simpkins, S. W.; et al. Massively Scaled-up Testing for SARS-CoV-2 RNA via Next-Generation Sequencing of Pooled and Barcoded Nasal and Saliva Samples. *Nat. Biomed. Eng.* **2021**, *5*, 657−665.

(7) Kim, J.; Park, J.; Park, S.; Seo, J.; Kwon, J.; Lee, H.; Kim, S.; Yang, H. Surface-Plasmonic-Field-Induced Photoredox Catalysis and Mediated Electron Transfer for Washing-Free DNA Detection. *Angew. Chem., Int. Ed.* **2020**, *59*, 19202−19208.

(8) Sridhara, S.; Goswami, H. N.; Whyms, C.; Dennis, J. H.; Li, H. Virus Detection via Programmable Type III-A CRISPR-Cas Systems. *Nat. Commun.* **2021**, *12*, 5653.

(9) Shen, Y. Z.; Zhang, N.; Sun, Y. D.; Zhao, W. W.; Ye, D. J.; Xu, J. J.; Chen, H. Y. Activatable QD-Based Near-Infrared Fluorescence Probe for Sensitive Detection and Imaging of DNA. *ACS Appl. Mater. Interfaces* **2017**, *9*, 25107−25113.

(10) Koebley, S. R.; Mikheikin, A.; Leslie, K.; Guest, D.; McConnell-Wells, W.; Lehman, J. H.; Al Juhaishi, T.; Zhang, X.; Roberts, C. H.; Picco, L.; Toor, A.; Chesney, A.; Reed, J. Digital Polymerase Chain Reaction Paired with High-Speed Atomic Force Microscopy for Quantitation and Length Analysis of DNA Length Polymorphisms. *ACS Nano* **2020**, *14*, 15385−15393.

(11) Sendroiu, I. E.; Gifford, L. K.; Lupták, A.; Corn, R. M. Ultrasensitive DNA Microarray Biosensing via in Situ RNA Transcription-Based Amplification and Nanoparticle-Enhanced SPR Imaging. *J. Am. Chem. Soc.* **2011**, *133*, 4271−4273.

(12) Foox, J.; Tighe, S. W.; Nicolet, C. M.; Zook, J. M.; Byrska-Bishop, M.; Clarke, W. E.; Khayat, M. M.; Mahmoud, M.; Laaguiby, P. K.; Herbert, Z. T.; Warner, D.; Grills, G. S.; Jen, J.; Levy, S.; Xiang, J.; Alonso, A.; Zhao, X.; Zhang, W.; Teng, F.; Zhao, Y.; et al. Performance Assessment of DNA Sequencing Platforms in the ABRF Next-Generation Sequencing Study. *Nat. Biotechnol.* **2021**, *39*, 1129−1140.

(13) Collie, G. W.; Parkinson, G. N.; Neidle, S.; Rosu, F.; De Pauw, E.; Gabelica, V. Electrospray Mass Spectrometry of Telomeric RNA (TERRA) Reveals the Formation of Stable Multimeric G-Quadruplex Structures. *J. Am. Chem. Soc.* **2010**, *132*, 9328−9334.

(14) Wang, D. M.; He, S. G.; Wang, X. H.; Yan, Y. Q.; Liu, J. Z.; Wu, S. M.; Liu, S. G.; Lei, Y.; Chen, M.; Li, L.; Zhang, J. L.; Zhang, L. W.; Hu, X.; Zheng, X. H.; Bai, J. W.; Zhang, Y. L.; Zhang, Y. T.; Song, M. X.; Tang, Y. G. Rapid Lateral Flow Immunoassay for the Fluorescence Detection of SARS-CoV-2 RNA. *Nat. Biomed. Eng.* **2020**, *4*, 1150−1158.

(15) Lin, M. H.; Wang, J. J.; Zhou, G. B.; Wang, J. B.; Wu, N.; Lu, J. X.; Gao, J. M.; Chen, X. Q.; Shi, J. Y.; Zuo, X. L.; Fan, C. H. Programmable Engineering of a Biosensing Interface with Tetrahedral DNA Nanostructures for Ultrasensitive DNA Detection. *Angew. Chem., Int. Ed.* **2015**, *54*, 2151−2155.

(16) Xue, T. Y.; Liang, W. Y.; Li, Y. W.; Sun, Y. H.; Xiang, Y. J.; Zhang, Y. P.; Dai, Z. G.; Duo, Y. H.; Wu, L. M.; Qi, K.; Shivananju, B. N.; Zhang, L. J.; Cui, X. Q.; Zhang, H.; Bao, Q. L. Ultrasensitive

Detection of miRNA with an Antimonene-based Surface Plasmon Resonance Sensor. *Nat. Commun.* **2019**, *10*, 28.
(17) Zhao, Y. X.; Chen, F.; Li, Q.; Wang, L. H.; Fan, C. H. Isothermal Amplification of Nucleic Acids. *Chem. Rev.* **2015**, *115*, 12491−12545.
(18) Wang, T.; Liu, Y.; Sun, H. H.; Yin, B. C.; Ye, B. C. An RNA-Guided Cas9 Nickase-Based Method for Universal Isothermal DNA Amplification. *Angew. Chem., Int. Ed.* **2019**, *58*, 5382−5386.
(19) Yao, C.; Tang, H.; Wu, W. J.; Tang, J. P.; Guo, W. W.; Luo, D.; Yang, D. Y. Double Rolling Circle Amplification Generates Physically Cross-Linked DNA Network for Stem Cell Fishing. *J. Am. Chem. Soc.* **2020**, *142*, 3422−3429.
(20) Chai, H.; Cheng, W. B.; Jin, D. Y.; Miao, P. Recent Progress in DNA Hybridization Chain Reaction Strategies for Amplified Biosensing. *ACS Appl. Mater. Interfaces* **2021**, *13*, 38931−38946.
(21) Duan, R. X.; Zuo, X. L.; Wang, S. T.; Quan, X. Y.; Chen, D. L.; Chen, Z. F.; Jiang, L.; Fan, C. H.; Xia, F. Lab in a Tube: Ultrasensitive Detection of MicroRNAs at the Single-Cell Level and in Breast Cancer Patients Using Quadratic Isothermal Amplification. *J. Am. Chem. Soc.* **2013**, *135*, 4604−4607.
(22) Hsieh, K.; Patterson, A. S.; Ferguson, B. S.; Plaxco, K. W.; Soh, H. T. Rapid, Sensitive, and Quantitative Detection of Pathogenic DNA at the Point of Care through Microfluidic Electrochemical Quantitative Loop-Mediated Isothermal Amplification. *Angew. Chem., Int. Ed.* **2012**, *51*, 4896−4900.
(23) Karunanayake Mudiyanselage, A. P. K. K.; Yu, Q. K.; Leon-Duque, M. A.; Zhao, B.; Wu, R.; You, M. X. Genetically Encoded Catalytic Hairpin Assembly for Sensitive RNA Imaging in Live Cells. *J. Am. Chem. Soc.* **2018**, *140*, 8739−8745.
(24) Chu, Y. X.; Wu, R.; Fan, G. C.; Deng, A. P.; Zhu, J. J. Enzyme-Free Photoelectrochemical Biosensor Based on the Co-Sensitization Effect Coupled with Dual Cascade Toehold-Mediated Strand Displacement Amplification for the Sensitive Detection of MicroRNA-21. *ACS Sustain. Chem. Eng.* **2018**, *6*, 11633−11641.
(25) Liu, X. Y.; Wang, H.; Deng, K. Q.; Kwee, S.; Huang, H. W.; Tang, L. Single Primer Based Multisite Strand Displacement Reaction Amplification Strategy for Rapid Detection of Terminal Deoxynucleotidyl Transferase Activity. *Anal. Chem.* **2019**, *91*, 7482−7486.
(26) Liang, C. P.; Ma, P. Q.; Liu, H.; Guo, X. G.; Yin, B. C.; Ye, B. C. Rational Engineering of a Dynamic, Entropy-Driven DNA Nanomachine for Intracellular MicroRNA Imaging. *Angew. Chem., Int. Ed.* **2017**, *56*, 9077−9081.
(27) Kamiya, Y.; Asanuma, H. Light-Driven DNA Nanomachine with a Photoresponsive Molecular Engine. *Acc. Chem. Res.* **2014**, *47*, 1663−1672.
(28) Zhao, J.; Li, Y. H.; Yu, M. M.; Gu, Z. J.; Li, L. L.; Zhao, Y. L. Time-Resolved Activation of pH Sensing and Imaging in Vivo by a Remotely Controllable DNA Nanomachine. *Nano Lett.* **2020**, *20*, 874−880.
(29) Cha, T. G.; Pan, J.; Chen, H. R.; Robinson, H. N.; Li, X.; Mao, C. D.; Choi, J. H. Design Principles of DNA Enzyme-Based Walkers: Translocation Kinetics and Photoregulation. *J. Am. Chem. Soc.* **2015**, *137*, 9429−9437.
(30) Brutzer, H.; Schwarz, F. W.; Seidel, R. Scanning Evanescent Fields Using a pointlike Light Source and a Nanomechanical DNA Gear. *Nano Lett.* **2012**, *12*, 473−478.
(31) Li, J. J.; Wang, W. J.; Zhang, H.; Lu, Z. C.; Wu, W. X.; Shu, M. B.; Han, H. Y. Programmable DNA Tweezer-Actuated SERS Probe for the Sensitive Detection of AFB1. *Anal. Chem.* **2020**, *92*, 4900−4907.
(32) Cheng, X. Y.; Bao, Y. F.; Liang, S.; Li, B.; Liu, Y. L.; Wu, H. P.; Ma, X. P.; Chu, Y. N.; Shao, Y.; Meng, Q.; Zhou, G. H.; Song, Q. X.; Zou, B. J. Flap Endonuclease 1-Assisted DNA Walkers for Sensitively and Specifically Sensing ctDNAs. *Anal. Chem.* **2021**, *93*, 9593−9601.
(33) Miao, P.; Tang, Y. DNA Walking and Rolling Nanomachine for Electrochemical Detection of miRNA. *Small* **2020**, *16*, 2004518.
(34) Pensa, E.; Cortés, E.; Corthey, G.; Carro, P.; Vericat, C.; Fonticelli, M. H.; Benítez, G.; Rubert, A. A.; Salvarezza, R. C. The Chemistry of the Sulfur-Gold Interface: In Search of a Unified Model. *Acc. Chem. Res.* **2012**, *45*, 1183−1192.
(35) Idili, A.; Vallée-Bélisle, A.; Ricci, F. Programmable pH-Triggered DNA Nanoswitches. *J. Am. Chem. Soc.* **2014**, *136*, 5836−5839.
(36) Chen, A. Y.; Gui, G. F.; Zhuo, Y.; Chai, Y. Q.; Xiang, Y.; Yuan, R. Signal-off Electrochemiluminescence Biosensor Based on Phi29 DNA Polymerase Mediated Strand Displacement Amplification for MicroRNA Detection. *Anal. Chem.* **2015**, *87*, 6328−6334.
(37) Xue, C.; Luo, M. X.; Wang, L.; Li, C. C.; Hu, S. Y.; Yu, X.; Yuan, P.; Wu, Z. S. Stimuli-Responsive Autonomous-Motion Molecular Machine for Sensitive Simultaneous Fluorescence Imaging of Intracellular MicroRNAs. *Anal. Chem.* **2021**, *93*, 9869−9877.
(38) Miao, P.; Ning, L. M.; Li, X. X. Gold Nanoparticles and Cleavage-Based Dual Signal Amplification for Ultrasensitive Detection of Silver Ions. *Anal. Chem.* **2013**, *85*, 7966−7970.
(39) Chai, H.; Miao, P. Bipedal DNA Walker Based Electrochemical Genosensing Strategy. *Anal. Chem.* **2019**, *91*, 4953−4957.

https://doi.org/10.1021/acsnano.1c11582
ACS Nano 2022, 16, 4726−4733